Bruchpilot Promotes Active Zone Assembly, Ca2+ Channel Clustering, and Vesicle Release

Robert J. Kittel, *et al.*

Science **312**, 1051 (2006);
DOI: 10.1126/science.1126308

Science (print ISSN 0036-8075; online ISSN 1095-9203) is published weekly, except the last week in December, by the American Association for the Advancement of Science, 1200 New York Avenue NW, Washington, DC 20005.

Bruchpilot Promotes Active Zone Assembly, Ca^{2+} Channel Clustering, and Vesicle Release

Robert J. Kittel,[1*] Carolin Wichmann,[1,2*] Tobias M. Rasse,[1*] Wernher Fouquet,[1] Manuela Schmidt,[1] Andreas Schmid,[1] Dhananjay A. Wagh,[3] Christian Pawlu,[2] Robert R. Kellner,[4] Katrin I. Willig,[4] Stefan W. Hell,[4] Erich Buchner,[3] Manfred Heckmann,[2]† Stephan J. Sigrist[1,5]†

The molecular organization of presynaptic active zones during calcium influx–triggered neurotransmitter release is the focus of intense investigation. The *Drosophila* coiled-coil domain protein Bruchpilot (BRP) was observed in donut-shaped structures centered at active zones of neuromuscular synapses by using subdiffraction resolution STED (stimulated emission depletion) fluorescence microscopy. At *brp* mutant active zones, electron-dense projections (T-bars) were entirely lost, Ca^{2+} channels were reduced in density, evoked vesicle release was depressed, and short-term plasticity was altered. BRP-like proteins seem to establish proximity between Ca^{2+} channels and vesicles to allow efficient transmitter release and patterned synaptic plasticity.

Synaptic communication is mediated by the fusion of neurotransmitter-filled vesicles with the presynaptic membrane at the active zone, a process triggered by Ca^{2+} influx through clusters of voltage-gated channels (*1*, *2*). The spacing between Ca^{2+} channels and vesicles at active zones is particularly thought to influence the dynamic properties of synaptic transmission (*3*).

The larval *Drosophila* neuromuscular junction (NMJ) is frequently used as a model of glutamatergic synapses (*4*, *5*). The monoclonal antibody Nc82 specifically stains individual active zones (fig. S1A) (*6*, *7*) by recognizing a coiled-coil domain protein of roughly 200 kD named Bruchpilot (BRP) (*6*). BRP shows homologies to the mammalian active zone components CAST [cytoskeletal matrix associated with the active zone (CAZ)–associated structural protein] (*8*), also called ERC (ELKS, Rab6-interacting protein 2, and CAST) (*9*). Whereas confocal microscopy recognized diffraction limited spots, the subdiffraction resolution of stimulated emission depletion (STED) fluorescence microscopy (*10*, *11*) revealed donut-shaped BRP structures at active zones (Fig. 1A). Viewed perpendicular to the plane of synapses, both single and multiple "rings" were uncovered, of similar size to freeze-fracture-derived estimates of fly active zones (*12*) (average length of isolated rings was 0.191 ± 0.002 μm, n = 204; average length of single rings of double ring structures was 0.148 ± 0.002 μm, n = 426; average length of double rings was 0.297 ± 0.005, n = 213) (fig. S1B). The donuts were up to 0.16 μm high, as judged by images taken parallel to the synaptic plane (Fig. 1A).

BRP seemed to demark individual active zones associated with clusters of Ca^{2+} channels. Transposon-mediated mutagenesis allowed

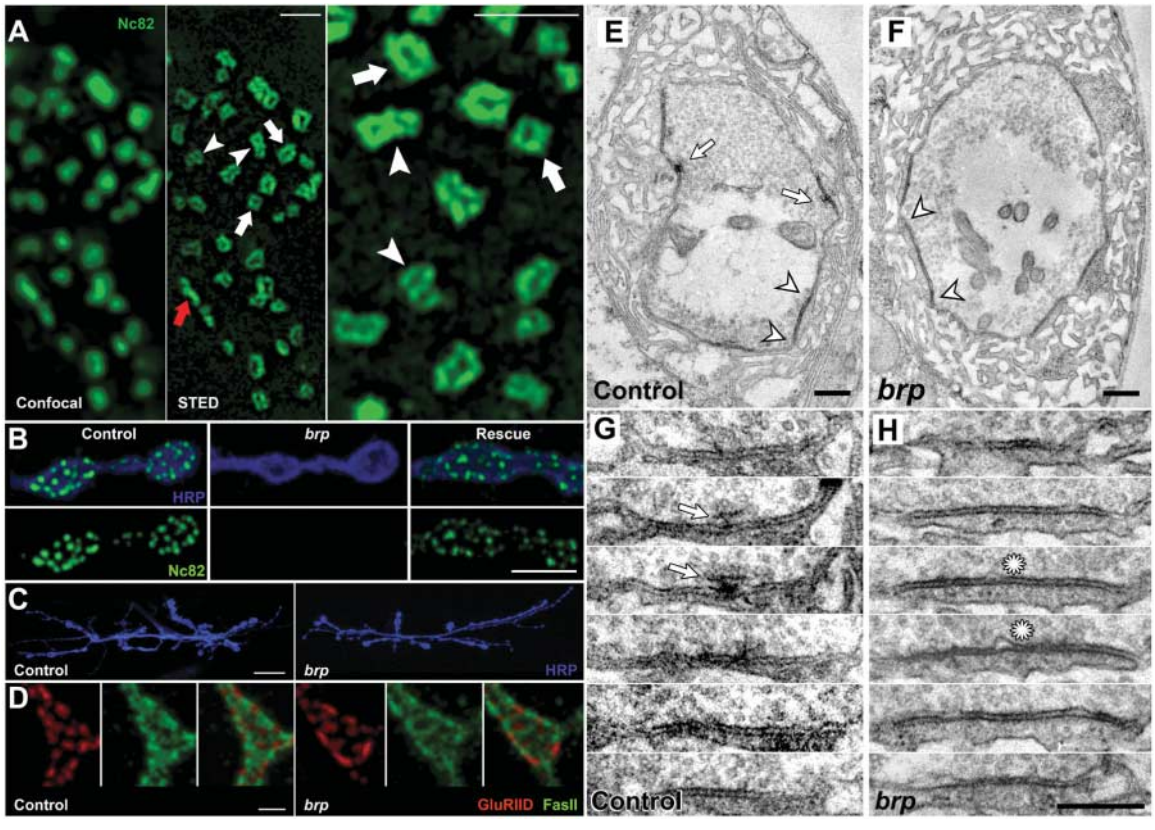

Fig. 1. Junctional and ultrastructural assembly in mutants of the active zone component BRP. (**A**) Unlike confocal, STED microscopy revealed donut-shaped structures recognized by Nc82. Viewed from above, both single (white arrows) and clusters of multiple rings (arrowheads) were identified. The red arrow indicates a synapse viewed parallel to the synaptic plane. (**B**) Individual synapses of control animals were labeled by Nc82, whereas *brp* mutant synapses completely lacked the Nc82 signal, which could be partially restored by re-expressing the *brp* cDNA in the *brp* mutant background with use of the neuron-specific driver line *ok6-GAL4*. (**C**) Staining with a neuronal membrane marker (anti–horseradish peroxidase) demonstrated normal morphological organization of *brp* NMJs. (**D**) Receptor fields were surrounded by the typical perisynaptic expression of the neuronal cell adhesion molecule (NCAM) homolog FasciclinII (FasII) in both *brp* mutants and controls. (A) to (D) are projections of confocal stacks. Scale bars represent in (A), 1 μm; (B), 4 μm; (C), 20 μm; and (D), 2 μm. (**E**) Electron micrograph of a control type Ib bouton with synapses (arrowheads) presynaptically decorated with T-bars (arrows). (**F**) A *brp* mutant bouton showing an overall normal organization but without T-bars. (**G**) Serial sections of a control synapse. A T-bar can be observed in two consecutive sections (arrows). (**H**) Serial sections of a representative *brp* mutant synapse completely lacking a T-bar and revealing presynaptic membrane rufflings (asterisks). Scale bars in (G) and (H), 250 nm.

us to isolate a mutant chromosome (brp^{69}) in which nearly the entire open reading frame of BRP was deleted (fig. S1C). *brp* mutants [brp^{69}/*df(2R)BSC29*] developed into mature larvae but did not form pupae. The Nc82 label was completely lost from the active zones of *brp* mutant NMJs but could be restored by re-expressing the *brp* cDNA (*6*) in the *brp* mutant background with use of the neuron-specific driver lines *ok6-GAL4* (Fig. 1B) or *elav-GAL4*. This also rescued larval lethality. Mutants had slightly smaller NMJs (average control size was 780.0 ± 35.8 μm², n = 14; average *brp* size was 593.3 ± 29.1 μm², n = 12; P = 0.0013) (Fig. 1C) and somewhat fewer individual synapses (average synapse number for control was 411.1 ± 41.5, n = 9; for *brp*, 296.3 ± 28.9; n = 8; P = 0.036). However, individual receptor fields, identified by the glutamate receptor subunit GluRIID (*13*), were enlarged in *brp* mutants (average field size in control was 0.43 ± 0.02 μm², n = 9; in *brp*, 0.64 ± 0.03 μm²; n = 8; P < 0.001) (Fig. 1D). Thus, principal synapse formation occurred in *brp* mutants, with individual postsynaptic receptor fields increased in size but moderately decreased in number.

In electron micrographs of *brp* mutant NMJs, synapses with pre- and postsynaptic membranes in close apposition were present at regular density (Fig. 1, F and H), and consistent with the enlarged glutamate receptor fields (Fig. 1D) postsynaptic densities appeared larger while otherwise normal (Fig. 1F). However, intermittent rufflings of the presynaptic membrane were noted (Fig. 1H), and *brp* mutants completely lacked presynaptic dense projections (T-bars). Occasionally, very little residual electron-dense material attached to the presynaptic active zone membrane was identified (fig. S2B). After re-expressing the BRP protein in the mutant background, T-bar formation could be partially restored (fig. S2C), although these structures were occasionally somewhat aberrant in shape. Thus, BRP assists in the ultrastructural assembly of the active zone and is essential for T-bar formation.

In *brp* mutant larvae we noted a drastic decrease in evoked excitatory junctional current (eEJC) amplitudes (Fig. 2A) by using two-electrode voltage clamp recordings of postsynaptic currents at low stimulation frequencies (*elav-GAL4* background control, –89.3 ± 3.4 nA; *brp*, –32.1 ± 5.9 nA; n = 10 each; P < 0.001; *ok6-GAL4* background control, –89.6 ± 4.4 nA; n = 9; *brp*, –32.8 ± 3.7 nA; n = 10; P < 0.001). This drop in current amplitude could be partially rescued through *brp* re-expression within the presynaptic motoneurons by using either *elav-GAL4* or *ok6-GAL4* (*elav-GAL4*, –55.5 ± 4.3 nA; n = 11; P = 0.01; *ok6-GAL4*, –62.2 ± 5.3 nA; n = 10; P = 0.002) (Fig. 2A). In contrast, the amplitude of miniature excitatory junctional currents (mEJCs) in response to single, spontaneous vesicle fusion events was increased over control levels (control, –0.84 ± 0.06 nA; *brp*, –1.17 ± 0.05 nA; n = 10 each; P = 0.004) (Fig. 2B). This is consistent with the enlarged individual glutamate receptor fields of *brp* mutants (Fig. 1D) and excludes a lack of postsynaptic sensitivity as the cause of the reduced eEJC amplitudes.

[1]European Neuroscience Institute Göttingen, Grisebachstrasse 5, 37077 Göttingen, Germany. [2]Institut für Klinische Neurobiologie, Josef Schneider Strasse 11, 97080 Würzburg, Germany. [3]Lehrstuhl für Genetik und Neurobiologie, Am Hubland, 97074 Würzburg, Germany. [4]Department of Nano-Biophotonics, Max Planck Institute for Biophysical Chemistry, Am Fassberg 11, 37077 Göttingen, Germany. [5]Institut für Klinische Neurobiologie, Rudolf Virchow Zentrum, 97080 Würzburg, Germany.

*These authors contributed equally to this work.
†To whom correspondence should be addressed. E-mail: Heckmann_M@klinik.uni-wuerzburg.de (M.H.); ssigris@gwdg.de (S.J.S.)

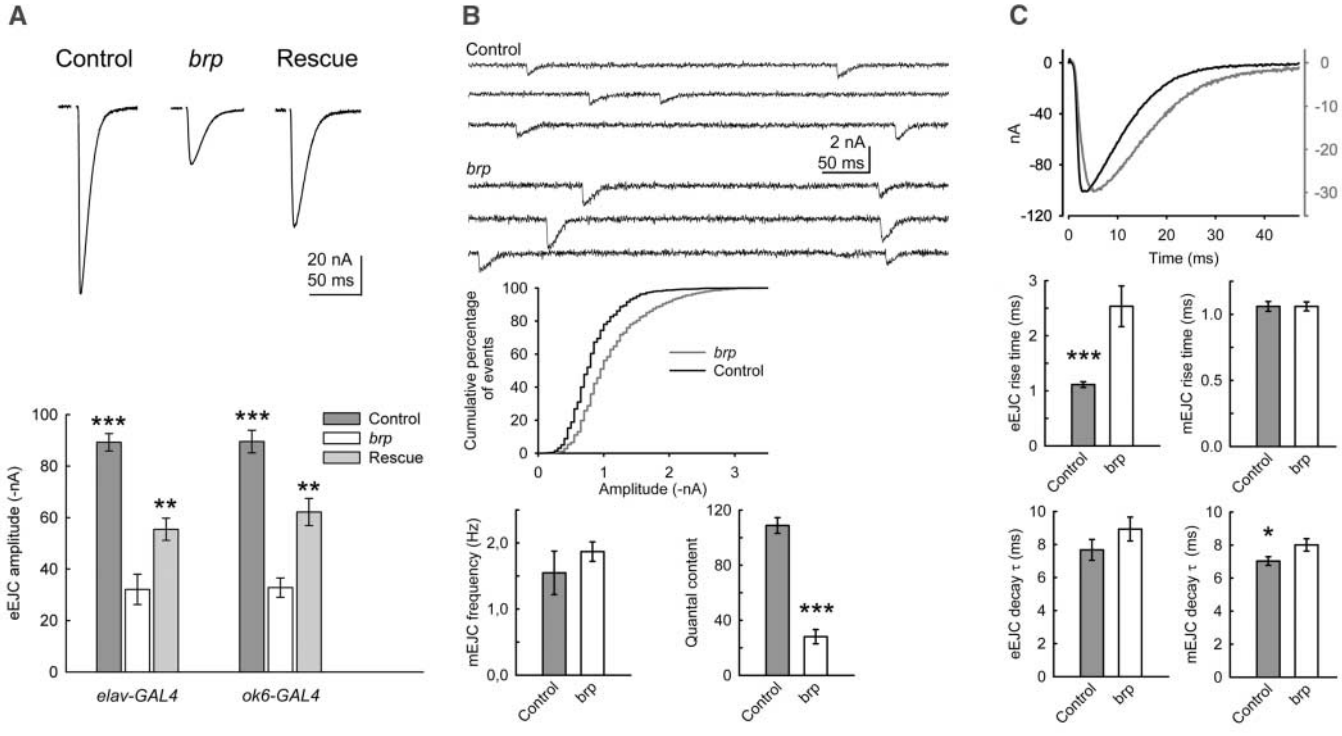

Fig. 2. Electrophysiological characterization of *brp* mutant NMJs. (**A**) (Top) Average traces of eEJCs at 0.2 Hz nerve stimulation and (bottom) mean eEJC amplitudes of control (dark gray), *brp* mutant (white), and rescued animals (light gray) carrying either a copy of *elav-GAL4* or *ok6-GAL4*. (**B**) Sample traces of mEJCs and a cumulative histogram of the amplitude distribution (0.05 nA bins). The average mEJC amplitude was increased in *brp* mutants, whereas the frequency was not significantly altered. Quantal content of *brp* NMJs was significantly reduced with respect to controls. (**C**) Average scaled eEJCs (control, black; *brp*, gray) illustrate the delayed release in *brp* mutants compared to controls. Although the rise time of eEJCs was significantly increased at *brp* NMJs, the rise time of mEJCs was indistinguishable from the control. The decay time constant (τ) of eEJCs was not significantly altered at *brp* synapses (τ control: 7.7 ± 0.6 ms; τ *brp*: 8.9 ± 0.7 ms; n = 10 each, P = 0.104), whereas mEJCs decayed with a slightly but significantly longer τ in the mutant than in the control (τ control: 7.0 ± 0.3 ms; τ *brp*: 8.0 ± 0.4 ms; n = 10 each, P = 0.045). One asterisk indicates $P \leq 0.05$, two asterisks, $P \leq 0.01$; and three asterisks, $P \leq 0.001$. Error bars indicate SEM.

It follows that the number of vesicles released per presynaptic action potential (AP) (quantal content) was severely compromised at *brp* mutant NMJs (control, 109 ± 5.7; *brp*, 28 ± 5.2; n = 10 each; $P < 0.001$) (Fig. 2B) and could not be attributed solely to the moderate decrease in synapse number. The ultrastructural defects of *brp* mutant synapses may interfere with the proper targeting of vesicles to the active zone membrane and thereby impair exocytosis. The number of vesicles directly docked to active zone membranes was slightly decreased in *brp* mutants (control average of 1.10 ± 0.13 from 51 active zones, n = 3; *brp* average of 0.87 ± 0.09 from 89 active zones, n = 4; P = 0.53). However, the amplitude distribution and sustained frequency of mEJCs (control, 1.55 ± 0.33 Hz; *brp*, 1.87 ± 0.15 Hz; n = 10 each; P = 0.186) (Fig. 2B) illustrated that *brp* mutant synapses did not appear to suffer from extrasynaptic release, as would be caused by a misalignment of vesicle fusion sites with postsynaptic receptors. Consistent with the appropriate deposition of exo- and endocytotic proteins, an apparently normal distribution of Syntaxin, Dap160, and Dynamin (fig. S3) was observed at *brp* mutant synapses.

The exact amplitude and time course of AP-triggered Ca^{2+} influx in the nerve terminal governs the amplitude and time course of vesicle release (*14*). Nerve-evoked responses of *brp* mutants were delayed (rise time of 2.53 ± 0.37 ms, n = 10) when compared with controls (rise time of 1.11 ± 0.05 ms, n = 10, $P < 0.001$), whereas in contrast mEJC rise times were unchanged (control, 1.06 ± 0.04 ms; *brp*, 1.06 ± 0.03 ms; n = 10 each) (Fig. 2C). Thus, evoked vesicle fusion events were less synchronized with the invasion of the presynaptic terminal by an AP. Spatiotemporal changes in Ca^{2+} influx have a profound effect on short-term plasticity (*15*–*17*). Whereas at 10 Hz controls (n = 18) exhibited substantial short-term depression of eEJC amplitudes, *brp* mutants (n = 15) showed strong initial facilitation before stabilizing at a slightly lower but frequency-dependent steady-state current (control at 10 Hz, –54.7 ± 3.3 nA; *brp*, –35.6 ± 3.0 nA; $P < 0.001$) (Fig. 3A). As judged by the initial facilitation at 10 Hz, neither a reduction in the number of releasable vesicles nor available release sites could fully account for the low quantal content of *brp* mutants at moderate stimulation frequencies. Furthermore, the altered short-term plasticity of *brp* mutant synapses suggested a change in the highly Ca^{2+}-dependent vesicle release probability (*18*). Paired-pulse protocols were applied to the NMJ (Fig. 3B). Closely spaced stimuli lead to a buildup of residual Ca^{2+} in the vicinity of presynaptic Ca^{2+} channels, enhancing the probability of a vesicle within this local Ca^{2+} domain to undergo fusion after the next pulse (*19*). The absence of marked facilitation at control synapses (ratio at 30-ms interval of 1.1 ± 0.03) could be explained by a depletion of release-ready vesicles (*20*). At *brp* mutant NMJs, however, the prominent facilitation at short interpulse intervals (ratio at 30-ms interval of 2.0 ± 0.13, $P < 0.001$) illustrated that the enhancement of release probability strongly outweighed the depletion of releasable vesicles. Thus, initial vesicle release probability was low, and release at *brp* synapses particularly benefited from the accumulation of intracellular Ca^{2+}.

Vesicle fusion is highly sensitive to the spacing between Ca^{2+} channels and vesicles at release sites (*3*). It has been calculated that doubling this distance from 25 to 50 nm decreases the release probability threefold (*21*), and the larger this distance, the more effective the slow synthetic Ca^{2+} buffer EGTA [ethyleneglycol-*bis*(β-aminoethyl)-*N*,*N*,*N*′,*N*′-tetraacetic acid] should become in suppressing release (*22*). Indeed, after bath application of membrane permeable EGTA-AM (tetraacetoxymethyl ester of EGTA), the reduction of evoked vesicle release was more pronounced at *brp* mutant than at control NMJs (control, 64.2 ± 13.8%; *brp*, 16.7 ± 8.8%; n = 6 each; P = 0.026) (Fig. 3C).

The Ca^{2+}-channel subunit Cacophony governs release at *Drosophila* NMJs (*23*, *24*). By using a fully functional, GFP (green fluorescent protein)–labeled variant (Cac^{GFP}) (*25*), we visualized Ca^{2+} channels in vivo (*26*). Consistently, Ca^{2+} channel expression was severely reduced over the entire NMJ and at synapses lacking BRP (Fig. 3D).

Thus, we conclude that *brp* mutants suffered from a diminished vesicle release probability

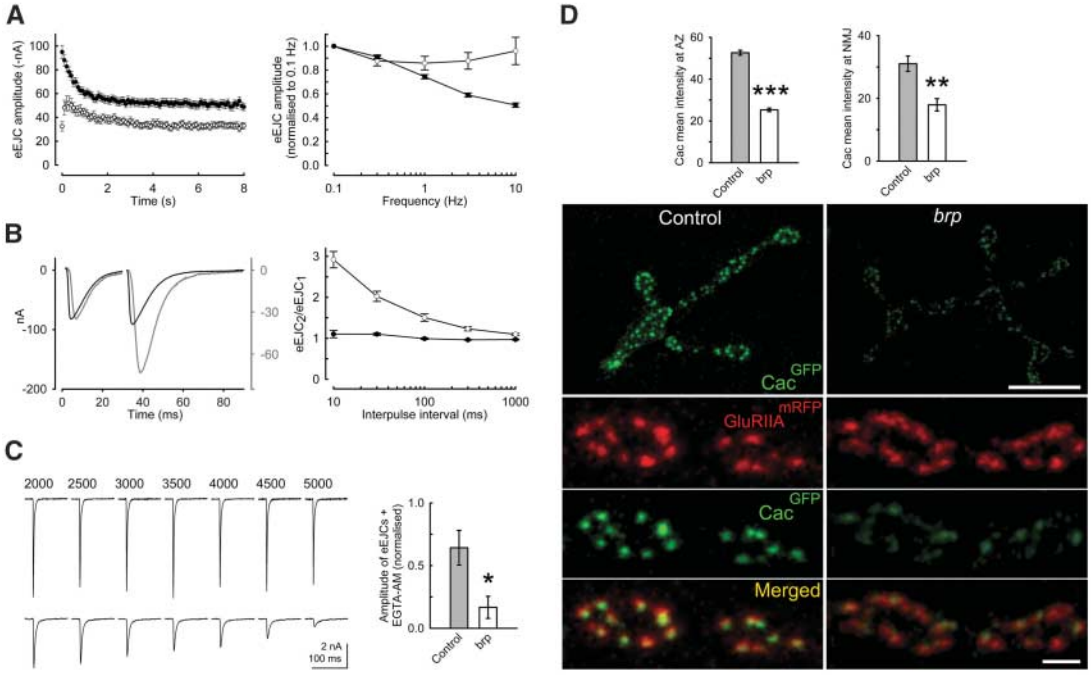

Fig. 3. Impaired vesicle release in *brp* mutants is caused by a mislocalization of presynaptic Ca^{2+} channels. (**A**) A 10-Hz stimulation revealed transient short-term facilitation of *brp* mutant currents (white circles) and the absence of a frequency-dependent depression of steady-state current amplitudes when compared with controls (black circles) ($n \geq 10$ per genotype at each frequency). (**B**) Average currents after paired-pulse stimulation at an interval of 30 ms normalized to the amplitude of the first pulse (control, black; *brp*, gray) and paired-pulse ratios at varying intervals demonstrate pronounced potentiation at *brp* NMJs (n = 9 per genotype at each interval). (**C**) Examples of nerve-evoked local postsynaptic currents recorded with a focal electrode (*36*, *37*) at indicated time points (in seconds) after bath application of EGTA-AM. The bar chart illustrates the severe reduction of current amplitudes in *brp* mutants 5000 s after EGTA-AM wash-in. The values are normalized to the initial eEJC amplitude. (**D**) Projections of confocal stacks displaying the NMJ (top images; scale bar, 10 μm) and several boutons (lower images; scale bar, 2 μm) reveal weak Cac^{GFP} signal at *brp* mutant synapses. Quantification of Cac^{GFP} intensity averaged over the entire NMJs [control, 31.1 ± 2.4 arbitrary units (a.u.); n = 13; *brp*, 18.0 ± 2.0 a.u.; n = 10; P = 0.0017] or only synaptic areas (control, 52.6 ± 1.2 a.u.; n = 421 synapses; *brp*, 25.3 ± 0.8 a.u.; n = 320 synapses; $P < 0.001$, student t test) included as bar charts. One asterisk indicates $P \leq 0.05$; two asterisks, $P \leq 0.01$; and three asterisks, $P \leq 0.001$. Error bars indicate SEM.

due to a decrease in the density of presynaptic Ca^{2+} channel clusters. It is conceivable that BRP tightly surrounds but is not part of the T-bar structure, contained within the unlabeled center of donuts. BRP may establish a matrix, required for both T-bar assembly as well as the appropriate localization of active zone components including Ca^{2+} channels, possibly by mediating their integration into a restricted number of active zone slots (*27*). Related mechanisms might underlie functional impairments of mammalian central synapses lacking active zone components (*28*) and natural physiological differences between synapse types (*17*). Electron microscopy has identified regular arrangements at active zones of mammalian CNS (central nervous system) synapses ("particle web") (*29*) and frog NMJs ("ribs") (*30*), where these structures have also been proposed to organize Ca^{2+} channel clustering. At calyx of Held synapses, both a fast and a slow component of exocytosis have been described (*31*). The fast component recovers slowly and is believed to owe its properties to vesicles attached to a matrix tightly associated with Ca^{2+} channels (*32*), whereas the slow component recovers faster (*31*) and is thought to be important for sustaining vesicle release during tetanic stimulation. In agreement with this concept, the absence or impairment of such a matrix at *brp* synapses has a profound effect on vesicle release at low stimulation frequencies, but this effect subsides as the frequency increases (Fig. 3A). The sustained frequency of mEJCs at *brp* synapses could be explained if spontaneous fusion events arise from the slow release component (*33*) or a pathway independent of evoked vesicle fusion (*34*).

Synapses lacking BRP and T-bars exhibited a defective coupling of Ca^{2+} influx with vesicle fusion, whereas the vesicle availability did not appear rate-limiting under low frequency stimulation. The activity-induced addition of presynaptic dense bodies has been proposed to elevate vesicle release probability (*35*). Our work supports this hypothesis and suggests an involvement of BRP or related factors in synaptic plasticity by promoting Ca^{2+} channel clustering at the active zone membrane.

References and Notes

1. R. G. Zhai, H. J. Bellen, *Physiology (Bethesda)* **19**, 262 (2004).
2. B. Katz, R. Miledi, *Proc. R. Soc. London Ser. B* **161**, 496 (1965).
3. E. Neher, *Neuron* **20**, 389 (1998).
4. H. L. Atwood, S. Karunanithi, *Nat. Rev. Neurosci.* **3**, 497 (2002).
5. Y. H. Koh, L. S. Gramates, V. Budnik, *Microsc. Res. Tech.* **49**, 14 (2000).
6. D. A. Wagh *et al.*, *Neuron* **49**, 833 (2006).
7. T. Wucherpfennig, M. Wilsch-Brauninger, M. Gonzalez-Gaitan, *J. Cell Biol.* **161**, 609 (2003).
8. T. Ohtsuka *et al.*, *J. Cell Biol.* **158**, 577 (2002).
9. Y. Wang, X. Liu, T. Biederer, T. C. Sudhof, *Proc. Natl. Acad. Sci. U.S.A.* **99**, 14464 (2002).
10. T. A. Klar, S. Jakobs, M. Dyba, A. Egner, S. W. Hell, *Proc. Natl. Acad. Sci. U.S.A.* **97**, 8206 (2000).
11. S. W. Hell, *Nat. Biotechnol.* **21**, 1347 (2003).
12. C. J. Feeney, S. Karunanithi, J. Pearce, C. K. Govind, H. L. Atwood, *J. Comp. Neurol.* **402**, 197 (1998).
13. G. Qin *et al.*, *J. Neurosci.* **25**, 3209 (2005).
14. E. F. Barrett, C. F. Stevens, *J. Physiol.* **227**, 691 (1972).
15. R. S. Zucker, W. G. Regehr, *Annu. Rev. Physiol.* **64**, 355 (2002).
16. H. L. Atwood, *Nature* **215**, 57 (1967).
17. A. Rozov, N. Burnashev, B. Sakmann, E. Neher, *J. Physiol.* **531**, 807 (2001).
18. J. S. Dittman, A. C. Kreitzer, W. G. Regehr, *J. Neurosci.* **20**, 1374 (2000).
19. B. Katz, R. Miledi, *J. Physiol.* **195**, 481 (1968).
20. H. von Gersdorff, R. Schneggenburger, S. Weis, E. Neher, *J. Neurosci.* **17**, 8137 (1997).
21. M. R. Bennett, L. Farnell, W. G. Gibson, *Biophys. J.* **78**, 2201 (2000).
22. E. M. Adler, G. J. Augustine, S. N. Duffy, M. P. Charlton, *J. Neurosci.* **11**, 1496 (1991).
23. F. Kawasaki, R. Felling, R. W. Ordway, *J. Neurosci.* **20**, 4885 (2000).
24. H. Kuromi, A. Honda, Y. Kidokoro, *Neuron* **41**, 101 (2004).
25. F. Kawasaki, B. Zou, X. Xu, R. W. Ordway, *J. Neurosci.* **24**, 282 (2004).
26. T. M. Rasse *et al.*, *Nat. Neurosci.* **8**, 898 (2005).
27. Y. Q. Cao *et al.*, *Neuron* **43**, 387 (2004).
28. W. D. Altrock *et al.*, *Neuron* **37**, 787 (2003).
29. G. R. Phillips *et al.*, *Neuron* **32**, 63 (2001).
30. M. L. Harlow, D. Ress, A. Stoschek, R. M. Marshall, U. J. McMahan, *Nature* **409**, 479 (2001).
31. T. Sakaba, E. Neher, *Neuron* **32**, 1119 (2001).
32. T. Sakaba, A. Stein, R. Jahn, E. Neher, *Science* **309**, 491 (2005).
33. J. Trommershauser, R. Schneggenburger, A. Zippelius, E. Neher, *Biophys. J.* **84**, 1563 (2003).
34. Y. Sara, T. Virmani, F. Deak, X. Liu, E. T. Kavalali, *Neuron* **45**, 563 (2005).
35. J. M. Wojtowicz, L. Marin, H. L. Atwood, *J. Neurosci.* **14**, 3688 (1994).
36. J. Dudel, *Pflugers Arch.* **391**, 35 (1981).
37. C. Pawlu, A. DiAntonio, M. Heckmann, *Neuron* **42**, 607 (2004).

38. We thank E. Neher for comments on the manuscript and C. Quentin for technical support. S.J.S. (SI 849/2-1, SFB406/A16, and Research Center for Molecular Physiology of the Brain Göttingen), M.H. (HE 2621/4-1), and E.B. and D.A.W. (SFB581/B6 and GRK200/3) were supported by the Deutsche Forschungsgemeinschaft; S.W.H., by the German Ministry of Research (BMBF); and T.M.R., by a Max Planck Fellowship. The European Neuroscience Institute Göttingen (ENI-G) is jointly funded by the Göttingen University Medical School, the Max Planck Society, and Schering AG.

Supporting Online Material

www.sciencemag.org/cgi/content/full/1126308/DC1
Materials and Methods
Figs. S1 to S3
References

16 February 2006; accepted 4 April 2006
Published online 13 April 2006;
10.1126/science.1126308
Include this information when citing this paper.

A Systems Approach to Mapping DNA Damage Response Pathways

Christopher T. Workman,[1]* H. Craig Mak,[1]* Scott McCuine,[1] Jean-Bosco Tagne,[2] Maya Agarwal,[1] Owen Ozier,[2] Thomas J. Begley,[3] Leona D. Samson,[4] Trey Ideker[1]†

Failure of cells to respond to DNA damage is a primary event associated with mutagenesis and environmental toxicity. To map the transcriptional network controlling the damage response, we measured genomewide binding locations for 30 damage-related transcription factors (TFs) after exposure of yeast to methyl-methanesulfonate (MMS). The resulting 5272 TF-target interactions revealed extensive changes in the pattern of promoter binding and identified damage-specific binding motifs. As systematic functional validation, we identified interactions for which the target changed expression in wild-type cells in response to MMS but was nonresponsive in cells lacking the TF. Validated interactions were assembled into causal pathway models that provide global hypotheses of how signaling, transcription, and phenotype are integrated after damage.

Exposure of cells to chemical and physical damaging agents can result in DNA lesions that contribute to the onset of cancer, aging, immune deficiencies, and other degenerative diseases (*1*). DNA damage is sensed by a highly conserved mechanism involving the ATM/ATR protein kinases in humans (ataxia-telangiectasia mutated/ataxia-telangiectasia and Rad3-related; homologous to Tel1 and Mec1 in yeast). These aggregate at DNA lesions (*2*) and activate signaling cascades that include the Chk protein kinases (Chk1, Rad53, and Dun1 in yeast). Chk kinases, in turn, trigger both transcriptional and transcription-independent responses, including activation of DNA repair machinery and cell-cycle arrest (*1*).

Beyond the known DNA repair genes, genomewide expression profiling in yeast has identified several hundred genes (*3*–*5*) whose expression is increased or decreased in response to alkylation damage by methyl-methanesulfonate (MMS). At the level of growth phenotype, sys-

[1]University of California San Diego, La Jolla, CA 92093, USA. [2]Whitehead Institute for Biomedical Research, Cambridge, MA 02139, USA. [3]University of Albany–State University at New York, Rensselaer, NY 12144, USA. [4]Massachusetts Institute of Technology, Cambridge, MA 02139, USA.

*These authors contributed equally to this work.
†To whom correspondence should be addressed. E-mail: trey@bioeng.ucsd.edu